2. D. M. McLean, *Cretaceous Res.* **6**, 235 (1985); C. B. Officer and C. L. Drake, *Science* **227**, 1161 (1985); V. E. Courtillot *et al., Earth Planet. Sci. Lett.* **80**, 361 (1986); V. E. Courtillot, *Isr. J. Earth Sci.* **43**, 255 (1994).
3. M. R. Rampino, S. Self, R. B. Stothers, *Annu. Rev. Earth Planet. Sci.* **16**, 73 (1988).
4. R. B. Stothers, J. A. Wolff, S. Self, M. R. Rampino, *Geophys. Res. Lett.* **13**, 725 (1986).
5. H. Sigurdsson, *Geol. Soc. Am. Spec. Pap. 247* (1990), p. 99.
6. D. M. Raup, *Science* **206**, 217 (1979); ——— and J. J. Sepkoski Jr., *ibid.* **231**, 833 (1986); D. H. Erwin, *Nature* **367**, 231 (1994).
7. D. H. Erwin, *Annu. Rev. Ecol. Syst.* **21**, 69 (1990); *The Great Paleozoic Crisis* (Columbia Univ. Press, New York, 1993).
8. G. J. Retallack, *Science* **267**, 77 (1995).
9. W. T. Holser and M. Magaritz, *Mod. Geol.* **11**, 155 (1987); *Geochim. Cosmochim. Acta* **56**, 3297 (1992). The notations $\delta^{13}C$ and $\delta^{34}S$ refer to $^{13}C/^{12}C$ and $^{34}S/^{32}S$ normalized to standard values, respectively.
10. J. J. Veevers, P. J. Conaghan, S. E. Shaw, *Geol. Soc. Am. Spec. Pap. 288* (1994), p. 187.
11. I. H. Campbell *et al., Science* **258**, 1760 (1992).
12. M. Javoy and V. Courtillot, *Earth Planet. Sci. Lett.* **94**, 409 (1989); M. Palmer, *Nature* **352**, 758 (1991).
13. P. R. Renne and A. R. Basu, *Science* **253**, 176 (1991).
14. G. B. Dalrymple *et al., Eos* **72**, 570 (1991); G. B. Dalrymple *et al., Geochim. Cosmochim. Acta* **59**, 2071 (1995).
15. F. M. Gradstein *et al., J. Geophys. Res.* **99**, 24051 (1994).
16. A. K. Baksi and E. Farrar, *Eos* **72**, 570 (1991).
17. P. R. Renne, *Earth Planet. Sci. Lett.* **131**, 165 (1995).
18. P. R. Renne *et al., Geology* **22**, 783 (1994).
19. J. C. Claoué-Long, Z. Zichao, M. Guogan, D. Shaohua, *Earth Planet. Sci. Lett.* **105**, 182 (1991).
20. Z. Zichao, *Phanerozoic Time Scale Bull. Liais. Inform. IUGS Subcomm. Geochronol.* **10**, 14 (1992).
21. Samples were prepared at the Yichang Institute of Geology and Mineral Resources. Inspection of the samples under a polarizing microscope indicated that each was >99% pure. Samples were irradiated at the Oregon State University Reactor (Corvallis, OR) for 60 hours along with Fish Canyon sanidine (28.03 Ma) and MMhb-1 hornblende (523.4 Ma) neutron fluence monitors as well as synthetic materials to monitor nucleogenic interfering Ar isotope ratios; the latter were identical to previously reported values (*17*). Approximately 5 to 10 mg of sample for each run was analyzed by incremental heating of multigrain separates with a defocused argon-ion laser, with the use of facilities and procedures described previously (*13, 17*). Individual crystals from each tuff were analyzed by laser total fusion [A. L. Deino and R. Potts, *J. Geophys. Res.* **95**, 8453 (1990)]. Uncertainties in dates are reported at the 2σ level as both internal errors (neglecting uncertainty in the age of the neutron fluence monitor) and external errors (including uncertainty in the age of the monitor). Both plateau dates and mean dates of individual grain analyses are inverse variance weighted means. The Meishan sanidine (C-2) was analyzed in 65 steps of incremental degassing (Fig. 2A) and yielded a plateau over more than 99% of the ^{39}Ar released. The uniform K/Ca, derived from $^{39}Ar_K/^{37}Ar_{Ca}$ (Fig. 2A), attests to the mineralogical purity of the sample. Our new plateau date is significantly younger than the previous $^{40}Ar/^{39}Ar$ plateau date of 255.7 ± 0.4 Ma (*20*), probably because the two dates are based on different neutron fluence monitors that have not been intercalibrated. Because the previous $^{40}Ar/^{39}Ar$ experiment was performed on a sample of >100 mg, it was more likely to have contained xenocrystic contamination, although our new single-crystal data indicate that such contamination is unlikely. Forty individual grains of C-2 sanidine were also analyzed by laser total fusion. Dates calculated from the individual analyses show a symmetric and unimodal distribution (Fig. 3A) with no evidence of xenocrystic contamination. The Shangsi plagioclase (GS-1) was run in duplicate, with 20 steps in the first analysis (GS-1.1) and 21 steps in the second (GS-1.2). Both runs yielded well-defined plateaus over ~95% of the ^{39}Ar released (Fig. 2, B and C); the plateau dates and internal errors were 250.08 ± 0.54 and 250.01 ± 0.48 Ma, and external errors were ±1.61 and ±1.59 Ma, respectively. Uniform Ca/K is evident in both samples (Fig. 2, B and C). A combined weighted mean of the two plateau dates was calculated because the results from the two runs were indistinguishable at the 95% confidence level. Thirty-eight individual grains of GS-1 plagioclase were also analyzed by laser total fusion (Fig. 3B). The single-grain dates are more dispersed than those of C-2 sanidine, and uncertainties in individual results are larger, because of lower ^{40}Ar and ^{39}Ar signals relative to system background levels, but again the distribution is unimodal and not suggestive of xenocrystic contamination.
22. J. C. Hudson and T. F. Anderson, *Trans. R. Soc. Edinburgh Earth Sci.* **80**, 183 (1989).
23. M. A. Richards and B. H. Hager, *J. Geophys. Res.* **89**, 5987 (1984).
24. C. G. Farnetani and M. A. Richards, *ibid.* **99**, 13813 (1994).
25. G. E. Birchfield, J. Weertman, A. T. Lunde, *Quat. Res.* **15**, 126 (1981); G. E. Birchfield and M. Ghil, *J. Geophys. Res.* **98**, 10385 (1993).
26. Y. Ricard *et al., Geophys. J. Int.* **113**, 284 (1993); M. A. Richards *et al., Eos* **75**, 64 (1994).
27. A. R. Basu *et al., Science* **269**, 822 (1995).
28. S. M. Stanley and X. Yang, *ibid.* **266**, 1340 (1994).
29. A. R. Basu *et al., ibid.* **261**, 902 (1993).
30. L. Zishun *et al., Sturdy on the Permian-Triassic Biostratigraphy and Event Stratigraphy of Northern Sichuan and Southern Shaanxi* (Geological Publishing House, Beijing, 1989).
31. S. Jin-zhang *et al., J. Fac. Sci. Hokkaido Univ. Ser. 4* **21**, 133 (1984); M. Ding, *Mem. Soc. Geol. Ital.* **34**, 263 (1986); K. Zhang, *Earth Sci. J. Wuhan Coll. Geol.* **12**, 193 (1987).
32. A. L. Deino and R. Potts, *Quat. Int.* **13**, 47 (1992).
33. Supported by NSF grants EAR-9496346 (P.R.R.), EAR-9117538 (M.A.R.), and EAR-9317214 (A.R.B.), the Ann and Gordon Getty Foundation (P.R.R. and M.T.B.), and the National Natural Science Foundation of China (Z.Z.). We thank T. A. Becker and W. D. Sharp for laboratory assistance and discussions and A. L. Deino, G. H. Curtis, and an anonymous reviewer for constructive reviews of the manuscript.

23 May 1995; accepted 12 July 1995

Short- and Intermediate-Range Structural Ordering in Glassy Boron Oxide

R. E. Youngman, S. T. Haubrich, J. W. Zwanziger,*
M. T. Janicke, B. F. Chmelka

Ordering at short-length scales is a universal feature of the glassy state. Experiments on boron oxide and other materials indicate that ordering on mesoscopic-length scales may also be universal. The high-resolution nuclear magnetic resonance (NMR) measurements of oxygen in boron oxide glass presented here provide evidence for structural units responsible for ordering on short- and intermediate-length scales. At the molecular level, planar $BO_{3/2}$ units accounted for the local ordering. Oxygen-17 NMR spectra resolved detailed features of the inclusion of these units in boroxol rings, oxygen bridging two rings, and oxygen shared between two nonring $BO_{3/2}$ units. On the basis of these and corroborative boron-11 NMR and scattering results, boron oxide glass consists of domains that are rich or poor in boroxol rings; these domains are proposed to be the structural basis of intermediate-range order in glassy boron oxide.

Inorganic network glasses such as B_2O_3 and SiO_2 lack long-range structural order, a physical property that differentiates them from analogous crystalline solids. However, glasses still have extensive short-range order (SRO) on length scales <5 Å, and some exhibit substantial intermediate-range order (IRO) at 5 to 20 Å (*1*). One such material is glassy boron oxide, B_2O_3, which consists of planar $BO_{3/2}$ groups (that is, each boron is bound to three oxygen atoms, each of which is bound to another boron atom). The majority of the $BO_{3/2}$ groups are part of six-member boroxol rings that are interconnected to the rest of the $BO_{3/2}$ network by bridging oxygen atoms (Fig. 1). The remaining $BO_{3/2}$ units are not part of rings. The boroxol ring is an example of what Elliott calls a superstructural unit, and it gives rise to IRO in this glass (*2*). Evidence for the boroxol ring structure has been obtained from neutron scattering (*3*), Raman spectroscopy (*4*), and NMR and nuclear quadrupole resonance (NQR) (*5, 6*). These experiments suggest that 70 to 80% of the boron is in the rings, which implies that the glass composition is a mixture of comparable amounts of boroxol rings and nonring $BO_{3/2}$ units. Bray and colleagues have also studied the oxygen sites in B_2O_3 glass, using continuous wave ^{17}O NMR (*7*). Their spectra could be fit to a two-site model, which is consistent with segregation of the oxygen between ring and nonring $BO_{3/2}$ units.

Recent light-scattering studies (*8, 9*) on a variety of glass formers, including B_2O_3, suggest that IRO is universal at the glass transition. Moynihan and Schroeder have proposed that the anomalous light-scattering at the glass transition arises from independently relaxing structural units of linear

R. E. Youngman, S. T. Haubrich, J. W. Zwanziger, Department of Chemistry, Indiana University, Bloomington, IN 47405, USA.
M. T. Janicke and B. F. Chmelka, Department of Chemical Engineering, University of California, Santa Barbara, CA 93106, USA.
*To whom correspondence should be addressed.

dimension 10 to 50 Å, which differ in density (8). A more complete picture of the nature of these regions has not been available but would provide crucial information on the atomic details of the glass transition in a network material (*10*). Remnants of these density fluctuations are to be expected below the glass transition, trapped in the structure of the static glass. Indeed, the boson peak in Raman spectra and the first sharp diffraction peak in the structure factor can both be interpreted in terms of IRO structures about 20 Å in size (*11, 12*).

In this report we present ^{17}O NMR results that resolve three distinct oxygen sites in B_2O_3, shedding new light on the origin of IRO in the glassy state. It is unusual for NMR to provide information on structures at mesoscopic-length scales; we succeeded in the present case by combining the ^{17}O spectra with previous high-resolution ^{11}B NMR data (5). In this way, detailed quantitative information was obtained on every resolvable site in the material, and site-to-site connectivities could be determined from the stoichiometry and simple counting arguments, using no adjustable parameters. The results show that the glass is composed of mesoscopic regions rich in boroxol rings and of regions consisting mainly of nonring $BO_{3/2}$ units, which together appear to account for the IRO in this material.

To obtain high-resolution ^{17}O NMR spectra of powdered glass samples, we used the technique of double rotation (DOR) (*13, 14*). DOR NMR removes the broadening due to both the chemical shift and to second-order quadrupole anisotropies of the central transition of quadrupolar nuclei with half-integer spin $I > ½$. The averaging is accomplished by rapid rotation of the axis of a spinning sample according to prescribed symmetry criteria, in this case icosahedral. The DOR experiment can be thought of as a double-axes analog of magic angle spinning (MAS). The resulting NMR spectrum consists of resonance peaks that are broadened only by the distributions of the isotropic chemical shift and quadrupole parameters. Because of the dependence of the second-order quadrupole interaction on the Larmor frequency, the isotropic chemical shift and quadrupolar contributions can be separated by performance of the DOR experiment at multiple fields (*15*).

To overcome the low natural abundance of ^{17}O, a sample of glassy B_2O_3, enriched to 21% in ^{17}O, was synthesized and used in this study (*16*). Figure 2 shows ^{17}O DOR NMR spectra (and accompanying simulations) of glassy B_2O_3 at fields of 8.4 and 11.7 T (*17*). The three resolved peaks are labeled to differentiate them from spinning sidebands, which occur at integral values of the outer rotor spinning speed and are easily identified by varying of the outer rotor spinning frequency. The isotropic shift of each peak is field dependent (Table 1), as are the splittings between pairs of peaks, indicating that their shifts are influenced significantly by second-order quadrupole effects (*15*). The field dependence also indicates that the three peaks arise from three structurally distinct oxygen sites. Using the shifts of the peaks in both fields, we determined the isotropic chemical shift $\delta_{iso}^{(CS)}$ and the quadrupole coupling product P_Q of the three different oxygen sites (Table 1) (*15*). The relative shifts of the peaks indicate that the upfield and downfield resonances remain identified with the same oxygen species at the two fields used here (*18*). The values for P_Q listed in Table 1 are similar to those found for bridging oxygen atoms in silicate glasses (*19, 20*) and are in good agreement with recent calculations (*21*), whereas the isotropic ^{17}O chemical shifts for B_2O_3 are downfield from those observed in silicates. The asymmetry η of the quadrupole interaction is estimated from simulations of the spectra to be $\eta = 0.9 \pm 0.1$ for each site (*22*).

Although the peak positions in the DOR spectra permit quantitative determination of the chemical shifts and quadrupole products, the noise level of the spectra and the large number of overlapping sidebands preclude accurate measurement of relative site populations from the integrated DOR peak areas. Under conditions of MAS, however, both of these difficulties are largely alleviated—the signal-to-noise ratio is significantly improved and the spinning sidebands have little or no overlap with the central transition (Fig. 3). Therefore, to determine the oxygen site populations, we used the interaction parameters for the three sites from the ^{17}O DOR data in simulations of the MAS spectra at the two magnetic fields. The simulations show good agreement with the experiments (Fig. 3). The relative oxygen populations are listed in Table 1; simulations of the ^{17}O DOR spectra using these populations are presented in Fig. 2 (*22*). Comparison between the simulated and experimental DOR spectra show that the main features are reproduced unambiguously; inclusion of additional simulation parameters, such as distributions of

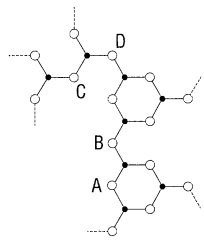

Fig. 1. Simple two-dimensional schematic diagram showing various possible arrangements of six-member boroxol rings and nonring $BO_{3/2}$ units. For this structure, there are four distinct types of oxygen atoms: A, oxygen contained within boroxol rings; B, oxygen bridging two boroxol rings; C, oxygen bridging two nonring $BO_{3/2}$ units; and D, oxygen bridging a boroxol ring and a nonring $BO_{3/2}$ unit. Open circles denote oxygen atoms and solid circles denote boron atoms. The dashed lines indicate nonspecific connections to the three-dimensional glassy network.

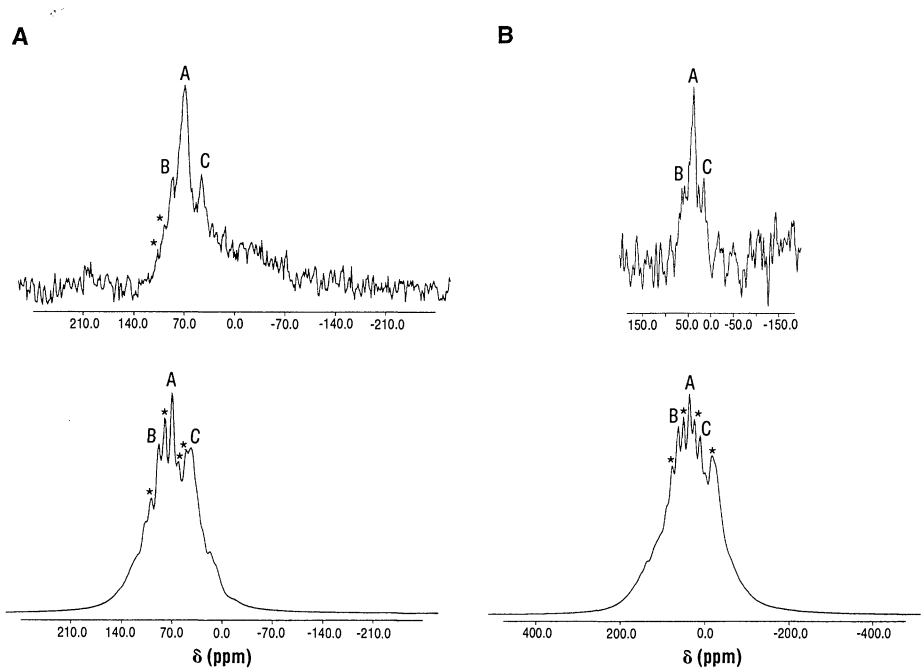

Fig. 2. ^{17}O DOR NMR spectra of B_2O_3 glass at two fields. Top panel of (**A**) shows spectrum at 11.7 T (67.6 MHz resonant frequency) and top panel of (**B**) shows spectrum at 8.4 T (48.8 MHz). Accompanying simulations are shown in bottom panels. Three resolved peaks are labeled A, B, and C to distinguish them from spinning sidebands, which are resolved for site B in spectrum (A). Simulations of the ^{17}O DOR NMR spectra were produced with the use of the site parameters listed in Table 1. Spinning sidebands due to the outer rotor frequency are denoted by asterisks. The shifts are referenced to $H_2^{17}O$.

quadrupole interactions and fluctuations in sample spinning frequencies, may improve the fits visually but not the confidence in the key quantitative findings. The important results obtained from the ^{17}O DOR spectra and simulations of glassy B_2O_3 are: (i) the existence of three distinct oxygen sites, (ii) determination of the quadrupole product and isotropic chemical shift associated with each type of oxygen, and (iii) that $\eta \approx 0.9$ for each site. In combination with the MAS data and simulations, these results provide a unique determination of the oxygen site populations.

To assign the three peaks in the ^{17}O NMR spectra, a model was used (Fig. 1) that included four distinct oxygen sites. The four oxygen sites are: A, oxygen in the six-member boroxol rings; B, oxygen bridging two of these boroxol rings; C, oxygen bridging two nonring threefold coordinate boron atoms; and D, oxygen linking a boroxol ring to a nonring $BO_{3/2}$ unit. Based on separate ^{11}B dynamic angle spinning (DAS) NMR results for this system (5), the fractions of boron in boroxol rings and in nonring $BO_{3/2}$ sites are 0.7 and 0.3, respectively.

To calculate the fraction of total oxygen at each type of site, we began with the bulk stoichiometry of the glass. Given that there are M boron atoms and N oxygen atoms, then for B_2O_3, $M/N = \frac{2}{3}$. Of the M boron atoms, R are in boroxol rings. The fraction in rings, from previous DAS measurements, is $R/M = 0.7$ (5). Because the number of oxygen atoms in boroxol rings, N_A, must equal the number of boron atoms in rings, the fraction of oxygen in rings is $N_A/N = 2R/3M = \frac{2}{3} \times 0.7 = 0.47$. This is consistent with the intensity shown in Table 1 for peak A. Note that the assignment of this peak depends only on the glass stoichiometry and the fraction of boron in rings, not on the presence or absence of any other type of oxygen site in the glass.

The R ring boron atoms provide $3R$ oxygen binding sites, of which $2R$ are occupied by oxygen in the rings. The remaining R oxygen binding sites are occupied by type B (ring-bridging-ring) and D (ring-bridging-nonring) oxygen species, of number N_B and N_D, respectively. B-type oxygen atoms use two such sites, because they bridge two rings, whereas D-type oxygen atoms use only one. Therefore

$$R = 2N_B + N_D \quad (1)$$

Likewise, the $(M - R)$ nonring boron atoms yield $3(M - R)$ oxygen binding sites. The N_C C-type (nonring-bridging-nonring) oxygen atoms use two of these sites each, whereas the N_D D-type species use one such site, leading to the additional relation

$$3(M - R) = 2N_C + N_D \quad (2)$$

Equations 1 and 2 relate N_B, N_C, and N_D, and the model can be solved parametrically in terms of any of the three variables—the solutions are equivalent. The solution in terms of N_D is shown in Fig. 4 along with the previously determined value of N_A/N, which is independent of N_D. The values of N_B/N and N_C/N are seen to differ by only six percentage points for all values of N_D, both decreasing as N_D increases. Our data show three resonances, the most intense of which has been assigned to the A site and has relative population 0.5. The remaining two resonances arise from sites with populations 0.2 and 0.3, and so on the basis of Fig. 4 are assigned to sites B and C, respectively, with a relatively small population in site D. This assignment is supported by the fact that a fourth site is not resolved. On the basis of the noise level of our spectra, we estimate $N_D/N \lesssim 0.1$.

Several alternative assignments should also be considered. Figure 4 shows that at $N_D/N \approx 0.25$, three resonances with about the correct intensities are also predicted. In this case, site B would be near the limit of detectability in DOR. But the small intensity difference between the B and C sites (Fig. 4) suggests that both will be seen, or neither; and again, no evidence was found for a fourth site in either the DOR or MAS spectra. Another alternative is that the fourth site lies directly under one of the observed resonances, which would distort the observed intensities. A possible candidate for such an overlap is the site A resonance, which is broader than the other resonances. Simulation of this effect (*23*), with the use of NMR parameters similar to those of the A-type oxygen and a site population of 10%, reproduced the observed width of the central resonance feature and

Table 1. NMR parameters for the three resolved oxygen sites in boron oxide glass. Isotropic shifts, chemical shifts, and P_Q were obtained from DOR NMR experiments at 8.4 and 11.7 T (Fig. 2). Population fractions were obtained from simulation of the MAS spectra with the use of these interaction parameters (Fig. 3).

Oxygen site	δ_{iso}^{obs} (8.4 T) (ppm)	δ_{iso}^{obs} (11.7 T) (ppm)	$\delta_{iso}^{(CS)}$ (ppm)	P_Q (MHz)	Population fraction
A	40 ± 1	71 ± 1	104 ± 5	5.0 ± 0.2	0.5 ± 0.1
B	65 ± 4	88 ± 1	113 ± 5	4.3 ± 0.2	0.3 ± 0.1
C	16 ± 4	46 ± 1	79 ± 5	5.0 ± 0.2	0.2 ± 0.1

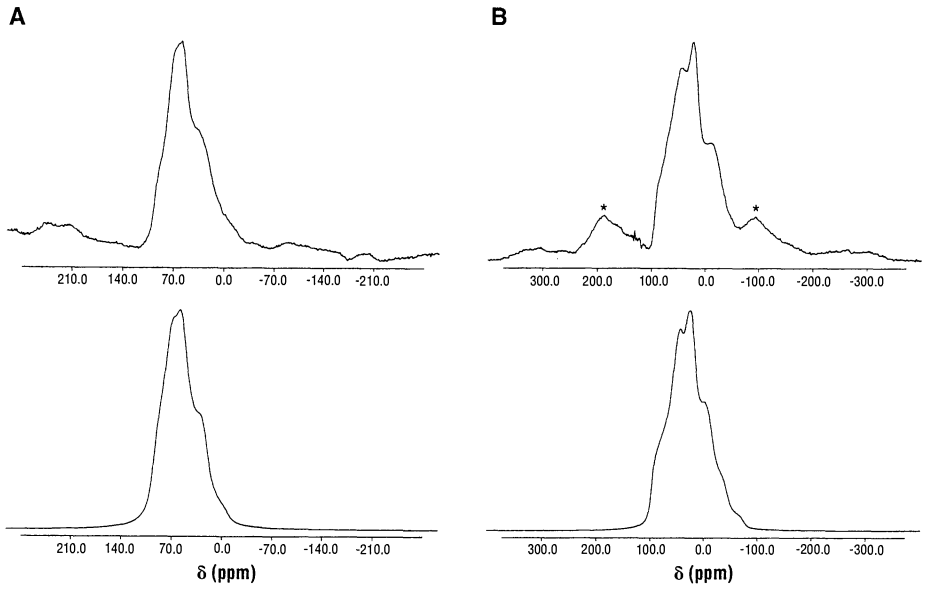

Fig. 3. ^{17}O MAS NMR spectra of B_2O_3 glass at two fields. Top panel of (**A**) shows spectrum at 11.7 T (67.6 MHz) and top panel of (**B**) shows spectrum at 8.4 T (48.8 MHz). Accompanying simulations are shown in bottom panels. They were done with the use of the same parameter set as in Fig. 2.

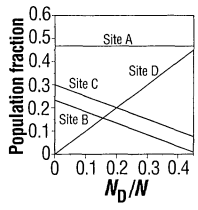

Fig. 4. The relative populations of the four oxygen sites (see Fig. 1 for labeling) as a function of the fraction of oxygen in site D. These follow directly from Eqs. 1 and 2 and from the fact that the fraction of oxygen in the ring sites (site A) is required to be 47%, on the basis of the fraction of boron in ring structures [70%; see (5)] and the stoichiometry of the glass.

increased its intensity in the simulation. Thus such overlapping resonances cannot be completely ruled out, but based on the data, they are expected to contribute no more than about 10% of the total intensity.

The isotropic chemical shifts of the observed ^{17}O resonances provide assignments for the B and C oxygen sites. As shown in Table 1, the A site (ring oxygen) has a chemical shift of 104 parts per million (ppm), whereas the remaining resonances have chemical shifts of 79 and 113 ppm. We assign the downfield resonance to site B, because this oxygen bridges two rings and is thus expected to have an electronic environment that is more similar to the rings themselves. The upfield resonance is assigned to site C, which bridges two nonring boron atoms. This assignment is consistent with the boron chemical shifts, for which the ring boron atoms are shifted downfield relative to the nonring boron atoms (*5, 21*). Boron shifts are unusual in that upfield shifts are produced by increased π backbonding to the boron atom (*24*). Thus the ring boron atoms are involved in relatively less backbonding, and so the oxygen atoms bonded to them (sites A and B) are relatively electron rich, leading to their downfield shifts (*24*). The nonring boron atoms experience more backbonding, so their partner oxygen atoms (site C) are electron poor, producing an upfield shift. The lack of ^{17}O NMR data on crystalline borates precludes more quantitative assignment.

This model for the structure of B_2O_3 glass thus assigns the three resonances in the ^{17}O NMR spectra to oxygen in boroxol rings, oxygen bridging two boroxol rings, and oxygen bridging two nonring boron sites. These results also indicate that the number of oxygen atoms connecting a boroxol ring with a nonring boron atom is small. This corresponds to a glassy network composed of boroxol ring–rich regions and nonring-rich regions, with some connectivity between the two that is below the threshold of detection in the present NMR studies.

The ring-rich and ring-poor microdomains proposed here are consistent with a variety of other probes of IRO in B_2O_3 glass. Anomalous light-scattering by B_2O_3 at the glass transition has been attributed to density fluctuations on the order of 10 to 50 Å (*8*). Applying the analysis of Duval *et al.* (*12*) to the boson peak in the Raman spectrum of B_2O_3 (*25*), we estimate a size of 30 Å for typical distinct regions in the glass. The size of the domains, according to the present model, can be estimated from the NMR data as follows: The volume and area of a boroxol ring, with connecting oxygen, are about 97 $Å^3$ and 21 $Å^2$, respectively, based on the bulk density. Assuming that rings on the surface of ring-rich regions are bound on average to one nonring $BO_{3/2}$ unit each, the number of surface boroxol rings N_S and the total number of rings N_R are related according to

$$\frac{N_A}{N_D} = \frac{3N_R}{N_S} \quad (3)$$

For a spherical region of radius r_d,

$$N_R = \frac{4}{3}\pi r_d^3/97\ Å^3\ \text{ring}^{-1} \quad (4)$$

and

$$N_S = 4\pi r_d^2/21\ Å^2\ \text{ring}^{-1} \quad (5)$$

Our experiments suggest that $N_D/N \lesssim 0.1$, and so also $N_A/N_D \gtrsim 4.5$. Combining this estimate with the above estimates for N_R and N_S leads to

$$r_d \gtrsim 21\ Å \quad (6)$$

for the sizes of the ring-rich domains, which is consistent with the aforementioned estimates of domain sizes in this material.

By using the high-resolution ^{17}O DOR NMR technique, we have resolved three distinct oxygen sites in glassy B_2O_3. These results, along with previous ^{11}B NMR studies, have been used to devise a structural model of B_2O_3 that consists of the formation of microdomains in the glassy network, which are rich or poor in boroxol rings. The average size of these regions is estimated to be 20 Å or greater, which is similar to the sizes estimated from light-scattering experiments and the boson peak observed in Raman spectra. Our results provide strong evidence that the ring-rich and ring-poor domains account for the structural origin of intermediate-range order in glassy B_2O_3.

REFERENCES AND NOTES

1. S. Elliott, *Physics of Amorphous Materials* (Longman, Essex, UK, ed. 2, 1990).
2. ———, *Nature* **354**, 445 (1991).
3. P. Johnson, A. Wright, R. Sinclair, *J. Non-Cryst. Solids* **50**, 281 (1982); A. Hannon, D. Grimley, R. Hulme, A. Wright, R. Sinclair, *ibid.* **177**, 299 (1994).
4. T. Bril, *Philips Res. Rep. Suppl.* **2**, 1 (1976); B. Meera and J. Ramakrishna, *J. Non-Cryst. Solids* **159**, 1 (1993).
5. R. E. Youngman and J. W. Zwanziger, *J. Non-Cryst. Solids* **168**, 293 (1994).
6. S. J. Gravina and P. J. Bray, *J. Magn. Reson.* **89**, 515 (1990).
7. G. E. Jellison Jr., L. W. Panek, P. J. Bray, G. B. Rouse Jr., *J. Chem. Phys.* **66**, 802 (1977).
8. C. Moynihan and J. Schroeder, *J. Non-Cryst. Solids* **160**, 52 (1993).
9. N. Bokov, *ibid.* **177**, 74 (1994).
10. The dynamics at the glass transition in a network material have been shown recently to involve breaking and reforming of network bonds [see I. Farnan and J. F. Stebbins, *Science* **265**, 1206 (1994)].
11. A. P. Sokolov, A. Kisliuk, M. Soltwisch, D. Quitmann, *Phys. Rev. Lett.* **69**, 1540 (1992).
12. E. Duval, A. Boukenter, T. Achibat, *J. Phys. Condens. Matter* **2**, 10227 (1990).
13. A. Samoson, E. Lippmaa, A. Pines, *Mol. Phys.* **65**, 1013 (1988); B. F. Chmelka and A. Pines, *Science* **246**, 71 (1989).
14. B. F. Chmelka and J. W. Zwanziger, in *NMR Basic Principles and Progress*, B. Blümich, Ed. (Springer-Verlag, Berlin, Germany, 1994), pp. 79–124.
15. The shift of a peak in a DOR spectrum can be expressed in parts per million as $\delta_{iso}^{obs} = \delta_{iso}^{(CS)} + \delta_{iso}^{quad}$, where $\delta_{iso}^{(CS)}$ is the usual isotropic chemical shift and δ_{iso}^{quad} is the isotropic shift due to second-order quadrupole effects. This latter term takes the form $\delta_{iso}^{quad} = -CP_Q^2/\upsilon_0^2$, where C is a a spin-dependent constant that for $I = 5/2$ (^{17}O) is $C = 6000$, and υ_0 is the I armor frequency in megahertz. P_Q is the quadrupole coupling product, which conveys information about the interaction between the quadrupole moment of the nucleus and the local electric field gradient. It has the form $P_Q = (e^2Qq/h)\sqrt{1 + \eta^2/3}$, with e^2Qq/h as the quadrupole coupling strength in megahertz, and η as the asymmetry of the electric field gradient tensor. The chemical shift and P_Q are extracted from DOR spectra by measurement of δ_{iso}^{obs} at two (or more) fields, thus varying υ_0, and solving simultaneously for $\delta_{iso}^{(CS)}$ and P_Q. The asymmetry η is determined from simulations of the spectra [see (*14*)].
16. We synthesized ^{17}O-enriched glassy B_2O_3 by first preparing boric acid from boron trifluoride etherate (Aldrich) and $H_2^{17}O$ enriched to 21.8 atomic % in ^{17}O (Icon Services, Summit, NJ). After dehydration of the boric acid under vacuum at 700°C for 2 hours, the glassy B_2O_3 was revitrified at 1000°C for an additional 5 min and quenched by removal of the platinum crucible from the furnace. The final water content of the glass was estimated to be approximately 0.5 mole percent [see T. J. M. Visser and J. M. Stevels, *J. Non-Cryst. Solids* **7**, 401 (1972)].
17. The NMR spectra were obtained with a Chemagnetics DOR probe head. All data were obtained with a typical inner rotor speed of 3.5 kHz and with outer rotor speeds in the range of 600 to 700 Hz. At 11.7 T, the data were obtained by signal averaging over 6400 acquisitions using 2-μs pulses and a recycle delay of 2 s. The data at 8.4 T were collected by averaging over 18,000 acquisitions using 2-μs pulses and a 4-s recovery delay.
18. The possibility of peaks B and C crossing on going from the high to low field is precluded by their isotropic shifts (Table 1); if they crossed, peak B would be required to shift downfield from 46 to 65 ppm as the field was reduced, which is physically unreasonable. The second-order quadrupole effect always induces an upfield shift that increases with decreasing field [see (*15*)].
19. X. Xue, J. F. Stebbins, M. Kanzaki, *Am. Miner.* **79**, 31 (1994).
20. I. Farnan *et al.*, *Nature* **358**, 31 (1992).
21. J. A. Tossell, *J. Non-Cryst. Solids* **183**, 307 (1995).
22. We did simulations by computing the time domain signal for each of the three sites, treating the central transition as an effective two-level system. The time-dependent signal was calculated under the assumption of a finite outer rotor frequency corresponding to the experimental value, and an infinite inner rotor frequency. The fact that we resolved only the outer rotor spinning sidebands and no inner rotor sidebands justifies this assumption. The interaction parameters in the simulations for each site were the isotropic chemical shift $\delta_{iso}^{(CS)}$, the quadrupole interaction strength e^2Qq/h, and the electric field gradient asymmetry η. The experimental value for $\delta_{iso}^{(CS)}$ was used, but from the shifts of the resonances in the DOR spectra it was not possible to determine e^2Qq/h and η separately, only $P_Q = (e^2Qq/h)\sqrt{1 + \eta^2/3}$. From simulations of the DOR and MAS spectra, we determined that $\eta = 0.9 \pm 0.1$ for all three sites. This value is larger than previous estimates (*7, 26*), which are not consistent with our data. We note also that models developed for silicates would suggest that $\eta = 0.9$ indicates a highly strained bond angle, but this prediction is not applicable to the present case because it explicitly excludes backbonding, an essential feature of boron-oxygen interactions. Simple models that include backbonding (*7*) predict that a bond angle change of only 1° produces a change of 0.1 in η, and so in borates, larger values of η do not lead to untenable structures. Finally, e^2Qq/h was determined from η and P_Q. The three signals computed this way, one for each site, were then scaled by the intensity factors determined from the MAS spectra, added, and Fourier-transformed to produce the results shown in Fig. 2.
23. R. E. Youngman, S. T. Haubrich, J. W. Zwanziger, M.

T. Janicke, B. F. Chmelka, data not shown.
24. P. Laszlo, Ed., *NMR of Newly Accessible Nuclei* (Academic Press, New York, 1983), vol. 2.
25. V. K. Malinovsky and A. P. Sokolov, *Solid State Commun.* **57**, 757 (1986).
26. J. A. Tossell and P. Lazzeretti, *J. Non-Cryst. Solids* **99**, 267 (1988).
27. The authors thank D. Lewis (Chemagnetics) for technical assistance with the DOR probe. J.W.Z. thanks U. Werner-Zwanziger for several helpful discussions. Supported by NSF under grant nos. DMR-9115787 (J.W.Z.), DMR-9222527 (B.F.C.), and DMR-9257064 (B.F.C.).

6 March 1995; accepted 26 June 1995

Branched Threadlike Micelles in an Aqueous Solution of a Trimeric Surfactant

Dganit Danino, Yeshayahu Talmon,* Hélène Levy, Gerard Beinert, Raoul Zana

Very long threadlike micelles observed in aqueous solutions of some surfactants have attracted much attention because of the peculiar rheological properties of these systems. Molecular dynamics simulations have suggested that branched threadlike micelles should exist in concentrated solutions of dimeric surfactants. Here experimental evidence, obtained from transmission electron microscopy at cryogenic temperature, is presented of branched threadlike micelles in aqueous solutions of a triquaternary ammonium (trimeric) surfactant made up of three amphiphilic moieties connected at the level of the headgroups by two propanediyl spacers.

Surfactants and, more generally, amphiphiles self-associate in water and form micelles, vesicles, and lyotropic liquid crystalline phases. Theory (*1*, *2*) predicts many possible micelle shapes of which only three have been found experimentally: spherical or spheroidal micelles, disk-shaped micelles, and elongated micelles (*3*). Elongated micelles come in a wide variety of forms: from short rigid rods to flexible "giant" micellar threads that are micrometers in length (*3*). Threadlike micelles usually develop from spheroidal micelles when a relevant system parameter is altered (*4*–*6*). This change of shape is well understood within the framework of existing theories (*1*, *2*). Thus, micelle growth from spherical to threadlike micelles takes place if the difference between the standard chemical potentials of the surfactant in the cylindrical part (μ^0_c) of an elongated micelle and in a spherical micelle (μ^0_s), $\Delta\mu^0 = \mu^0_c - \mu^0_s$, is negative. Values of $\Delta\mu^0$ as low as -0.1 to $-0.2k_BT$ (where k_B is Boltzmann's constant and T is temperature) are sufficient to bring about an enormous micellar growth (*5*).

Transmission electron microscopy at cryogenic temperature has been extensively used to obtain direct visualization of threadlike micelles in aqueous solutions of pure conventional surfactants and of surfactant mixtures (*3*, *4*, *7*). Dimeric surfactants, made up of two identical amphiphilic moieties [$C_mH_{2m+1}(CH_3)_2N^+$ Br^-] connected at the level of the charged nitrogen atoms by a polymethylene spacer $(CH_2)_s$, have been found to form very long threadlike micelles at relatively low concentrations of 1% or less, provided the spacer is short enough (*8*).

Recently the possible existence of cross-links, connections, or seams between long and entangled threadlike micelles attracted much interest (*2*, *5*, *9*, *10*). Such cross-links would result in the formation of connected networks of elongated micelles, which are likely to have interesting rheological properties. Several experiments led to the postulation of the existence of such networks (*2*, *5*, *9*). Drye and Cates (*10*) investigated theoretically the formation of cross-links between threadlike micelles. They concluded that for conventional surfactants the free energy cost for forming a cross-link is much higher than for forming a hemispherical end-cap terminating a cylindrical micelle. This is because the surfactant layer at the seam between two branches is concave, whereas it is convex in the cylindrical part of the micelle, where the layer curvature is essentially equal to the spontaneous curvature. Therefore, a seam forms only when the system contains almost no end-caps, that is, when the micelles are extremely long (*10*). This is probably the case at the very high salt concentration at which some of the abovementioned experiments were performed.

Molecular dynamics simulations of aqueous solutions of dimeric surfactants have accounted for the formation of elongated micelles. They also predicted that these elongated micelles should be branched or cross-linked (*11*). Furthermore, the simulations showed that the two alkyl chains of a given dimeric surfactant are radially oriented and roughly parallel in the cylindrical parts of the branched micelles; however, they are almost perpendicular when the surfactant molecule is located at a seam between two branches, with one chain oriented radially with respect to one branch and the other oriented radially with respect to the other branch (*12*). This very peculiar packing of the chains probably decreases the free energy cost associated with the formation of connections between threadlike micelles to a value that must be comparable to that of forming hemispherical end-caps which terminate elongated micelles. Thus, dimeric surfactants and their higher homologs trimeric surfactants potentially provide an easier way to obtain connected or branched threadlike micelles.

Here we present transmission electron micrographs taken at cryogenic temperatures showing branching in the threadlike micelles formed by a triquaternary ammonium tribromide (trimeric) surfactant that we synthesized and purified (*12*). Molecular dynamics simulations have not been performed yet for trimeric surfactants. It is likely, however, that the mechanism of reduction of the free energy cost for forming a seam holds and is even amplified with trimeric surfactants.

The trimeric surfactant we synthesized and purified (*12*), which is referred to as 12-3-12-3-12 following the terminology previously used (*8*, *12*, *13*), is shown in Scheme 1. This surfactant can be formally

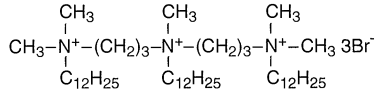

Scheme 1.

considered as the trimer of the conventional surfactant dodecyltrimethylammonium bromide, which forms only spheroidal micelles even at fairly high concentration and ionic strength.

A 2% aqueous solution of the trimeric surfactant was studied by transmission electron microscopy at cryogenic temperatures (cryo-TEM). Thin vitreous samples were prepared under controlled temperature and 100% relative humidity as previously described (*8*). Some representative micrographs are shown in Fig. 1. A very long threadlike micelle is seen in the center of Fig. 1A. The featureless background is vitreous ice. In the central area of the field of view no overlap of micelles has occurred; thus, the branching of this long micelle (marked by arrow heads) can be easily seen. The clarity of the images of the meeting points of the three segments at each branching point strongly suggests that these are true branches. Furthermore, it is highly unlikely that the numerous branching points seen in

D. Danino and Y. Talmon, Department of Chemical Engineering, Technion-Israel Institute of Technology, Haifa 32000, Israel.
H. Levy, G. Beinert, R. Zana, Institut C. Sadron, 6 Rue Boussingault, 67000 Strasbourg, France.

*To whom correspondence should be addressed.